



Article

Electronic and Magnetic Properties of FeCl₃ Intercalated Bilayer Graphene

Jiajun Dai *, Shilpa Yadav and Beate Paulus *

Institut für Chemie und Biochemie, Freie Universität Berlin, Arnimallee 22, 14195 Berlin, Germany; shiy99@zedat.fu-berlin.de

* Correspondence: daij96@zedat.fu-berlin.de (J.D.); b.paulus@fu-berlin.de (B.P.)

Abstract: Graphene has gained significant attention since its discovery in 2004, and the modification of few-layer graphene provides a platform to tailor its physical and electronic properties. In this study, we employed unrestricted density functional theory (DFT) with the PBE+U functional to investigate the electronic and magnetic properties of FeCl₃-intercalated bilayer graphene (BLG). Both in BLG and stage-2 intercalated graphite, a distinct localization of electrons on a specific Fe atom is evident, gaining approximately 0.245 electrons evaluated with Bader analysis, while the holes are delocalized within the graphene layers. This results in p-doped graphene, characterized by a shift of the Dirac cone by 0.74 eV for BLG and 0.70 eV for stage-2 intercalated graphite. Ferromagnetic ordering is observed within the plane of FeCl₃-intercalated BLG, whereas the FeCl₃ layers exhibit antiferromagnetic coupling in stage-2 intercalated graphite. The ferromagnetic nature and electronic structure of the FeCl₃-intercalated BLG is retained under pressure.

Keywords: bilayer graphene (BLG); FeCl₃; density functional theory (DFT); intercalation; magnetic property; doping

1. Introduction

Graphite intercalation compounds (GICs) [1,2] have attracted considerable attention due to their distinct properties arising from the introduction of intercalants into graphite host materials [3,4]. These intercalants encompass a range of materials, including well-known alkali and earth metals, as well as metal oxides, metal chlorides, acidic oxides, fluorides, and oxyhalides [5–7]. Since the concept of GICs was first introduced in 1841, these compounds have been extensively studied [8] and characterized using diverse methods. The unique structural, magnetic, electronic, and optical properties of GICs have paved the way for their applications in various fields, including electrodes in batteries, fuel cells, and catalysis [9].

On the other hand, a monolayer of graphite, called graphene [10], has gained significant attention due to its remarkable properties and the presence of Dirac fermion-like charge carriers [11]. In recent years, substantial progress has been made in graphene research, and various methods [12,13] have been explored to customize its electronic and structural characteristics. Due to the high surface-to-bulk ratio inherent in two-dimensional systems, few-layer graphene (FLG) intercalation offers opportunities to explore novel chemical and physical phenomena [14–17]. Unlike bulk GICs, FLG exhibits unique properties [18] due to the presence of surface boundaries, which disrupt the translational symmetry perpendicular to the graphene layers. By hybridizing FLG with other molecules through chemical or physical reactions, the properties of FLG can be tailored and utilized in various applications [19,20]. Among the FLG family, bilayer graphene (BLG) intercalation compounds have garnered particular interest due to their diverse magnetic and superconducting properties, providing a platform to investigate long-range ordered phenomena in two-dimensional systems [21,22].



Citation: Dai, J.; Yadav, S.; Paulus, B. Electronic and Magnetic Properties of FeCl₃ Intercalated Bilayer Graphene. *C* **2023**, *9*, 95. <https://doi.org/10.3390/c9040095>

Academic Editors: Vardan Apinyan and Tadeusz K. Kopeć

Received: 2 August 2023

Revised: 20 September 2023

Accepted: 26 September 2023

Published: 3 October 2023



Copyright: © 2023 by the authors. Licensee MDPI, Basel, Switzerland. This article is an open access article distributed under the terms and conditions of the Creative Commons Attribution (CC BY) license (<https://creativecommons.org/licenses/by/4.0/>).

Intercalant FeCl₃ [23] stands out from many other GICs due to its relative stability in open-air environments, which has attracted continuous research interest [24,25]. A Hall bar device [26] utilizing FeCl₃-intercalated graphite has been successfully fabricated, demonstrating a high carrier density exceeding 10¹³ cm⁻², indicating its potential for environmentally stable utilization as electrical conductor. The strong charge transfer effect between the carbon atomic layers and FeCl₃ significantly modifies the band structure of graphite, resulting in p-type doping for different stages of intercalation [27,28]. Zhan et al. successfully prepared FeCl₃ intercalated few-layer graphene (FLG) using a two-zone vapor transport method [29]. Despite the potential applications of FeCl₃-intercalated bilayer graphene [30], comprehensive research on its magnetic and electronic properties is scarce. Gaining a thorough understanding of these properties is essential, as it can provide valuable insights into the potential applications of this system. Li et al. [31] investigated the structural, electronic, and magnetic properties of stage-1 and -2 FeCl₃-based GICs in the framework of the GGA+U implementation of DFT. By applying the experimental lattice parameters, their calculation results are in agreement with the experimental findings, in which stage-1 shows antiferromagnetic ordering below 3.6 K and stage-2 displays ferromagnetic ordering below 8.5 K [7]. Kim et al. [26] investigated the electronic properties of FeCl₃-intercalated BLG using the fixed interlayer distance of the value of bulk GIC, 0.94 nm. Their DFT+U calculations predict the Fermi level shift of around 0.6 eV and charge transfer of around 0.01 eV per C atom. However, there is no prior research that has conducted a full optimization of lattice parameters and structures while considering the influence of the dispersion interactions.

In this study, we want to extend the already existing first-principles calculations to investigate the magnetic and electronic properties of FeCl₃-intercalated BLG with different stacking patterns. The calculations were performed using the unrestricted PBE+U functional, and dispersion interactions were considered. Our results reveal that both in BLG and stage-2 intercalated graphite, a distinct localization of electrons on a specific Fe atom is evident, gaining approximately 0.245 electrons, while the holes are delocalized within the graphene layers. Moreover, we have explored the effect of uniaxial pressure applied perpendicular to the two-dimensional (2D) system on the magnetic states and electronic properties of FeCl₃-intercalated BLG.

2. Computational Detail

The spin-polarized DFT calculations based on plane-wave basis sets were performed with the Vienna *ab initio* simulation package (VASP) [32,33]. The Perdew–Burke–Ernzerhof (PBE) exchange–correlation functional [34] was employed. The ion-cores were described by projector-augmented-wave (PAW) potentials [35] and the valence electrons (Fe (3*d*, 4*s*), Cl (3*s*, 3*p*) and C (2*s*, 2*p*)) were described by plane waves associated with kinetic energies of up to 500 eV. Brillouin-zone integration was performed on Γ -centered symmetry with Monkhorst-Pack meshes by the tetrahedron method with Blöchl corrections [36]. The $3 \times 3 \times 1$ *k*-mesh was used for the structure optimization. The DFT+*U* scheme [37,38] was adopted for the treatment of Fe 3*d* orbitals, with the parameter $U_{\text{eff}} = U - J$ equal to 4 eV [31]. Dispersion interactions were considered by Grimme’s D3 parameterisation [39]. The charges of individual atoms are calculated by performing Bader charge analysis [40].

When modeling the FeCl₃-intercalated BLG, a supercell with 5×5 units of graphene hexagonal primitive cell and 2×2 units of one layered FeCl₃ primitive cell ($R\bar{3}$ space group) was constructed. A vacuum gap was set to approximately 30 Å. During structure optimization, the convergence criteria for energy and force were set equal to 10⁻⁵ eV and 10⁻² eV/Å, respectively. Phonon calculations were performed at the gamma point, showing that the FeCl₃ structure yields only positive frequencies. This result indicates the structural stability of intercalated FeCl₃.

The binding energy of FeCl₃-intercalated BLG system is defined as follows:

$$\Delta E_{\text{bind}} = E_{\text{total}} - E_{\text{FeCl}_3} - E_{\text{BLG}}, \quad (1)$$

where E_{total} represents the total energy of the FeCl_3 -intercalated BLG system, E_{FeCl_3} is the total energy of the 2×2 units of one-layer FeCl_3 primitive cell, and E_{BLG} is the total energy of 5×5 units of AA or AB stacking BLG.

The intercalation energy of stage-2 GICs system is defined as follows:

$$\Delta E_{\text{int}} = E_{\text{total}} - E_{\text{FeCl}_3} - E_{\text{graphite}}, \quad (2)$$

where E_{total} represents the total energy of the stage-2 GICs system, E_{FeCl_3} is the total energy of the 2×2 units of layered FeCl_3 primitive cell, and E_{graphite} is the total energy of 5×5 units of AB stacking graphite (per unit cell containing two carbon layers).

3. Results

3.1. Structural Properties

As shown in Figure 1, two stacking patterns (AA stacking and AB stacking) and two magnetic configurations (ferromagnetic (FM) and antiferromagnetic (AFM)) were considered when performing the structural optimization of FeCl_3 -intercalated BLG. A supercell consisting of 5×5 graphene primitive cell and 2×2 layered FeCl_3 primitive cell was constructed to reduce the lattice mismatch. During the optimization of the lattice parameter and structure, lattice constant c was fixed to 30 \AA for the system to avoid the interaction between adjacent periodic structure.

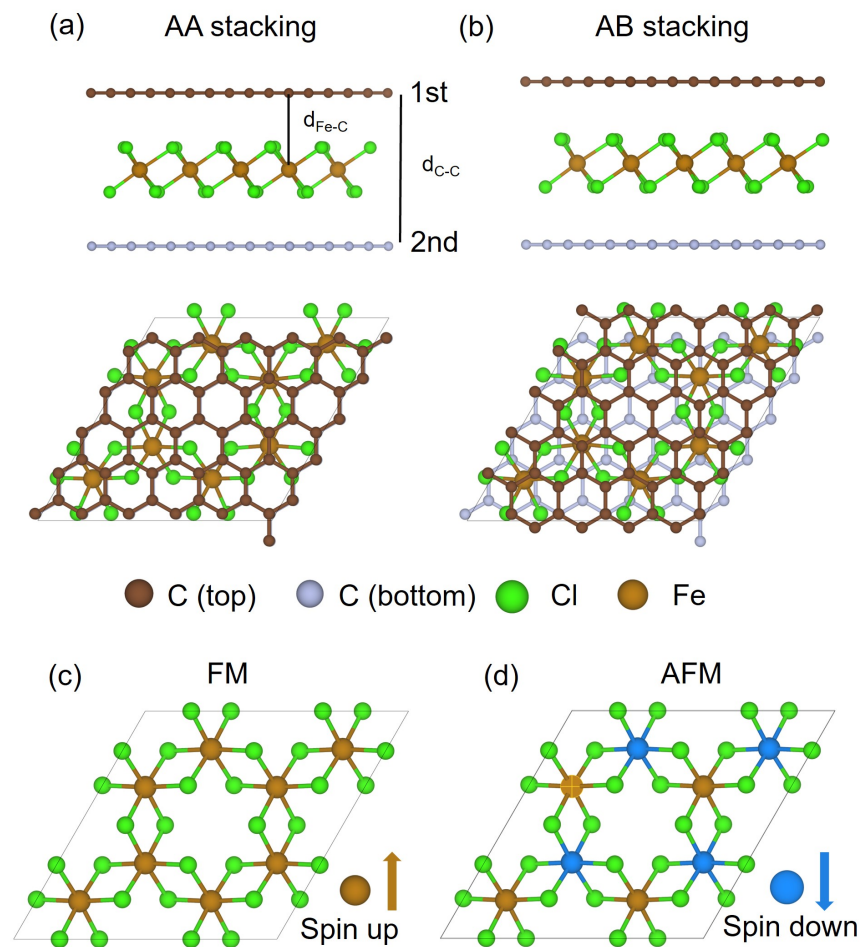


Figure 1. Schematic diagram illustrating the stacking patterns (a) AA stacking, (b) AB stacking and magnetic configuration, (c) ferromagnetic (FM), (d) antiferromagnetic (AFM).

Table 1 presents the calculated properties of FeCl_3 -intercalated BLG. The optimized lattice constant a was found to be approximately 12.33 \AA for all the investigated structures,

resulting in a lattice mismatch of 0.1% for graphene and 1.2% for FeCl₃. Notably, FM configuration of FeCl₃-intercalated BLG with AA stacking patterns exhibited the lowest energy. The binding energy ($\Delta E_{\text{binding}}$) was calculated to be -2.98 eV, corresponding to an energy of -0.373 eV per FeCl₃ unit, suggesting a favorable binding between FeCl₃ and the graphene layers.

Table 1. Calculated properties of graphene, BLG, graphite, FeCl₃ monolayer, FeCl₃-intercalated BLG and FeCl₃-intercalated graphite: lattice constant referring to 5×5 graphene supercell (Å), energy of the system (eV), binding energy (ΔE_{bind}) or intercalation energy (ΔE_{int}) per two layers of 5×5 graphene and one layer of 2×2 FeCl₃, magnetic momentum (μ_B), the average distance between C atomic layers (Å), the change in the z-coordinate of carbon atoms within both upper and lower carbon atomic layers (Å), and charge transfer occurring from graphene to FeCl₃ (e).

Material	Stacking Pattern	Magnetic Configuration	Lattice Constant a (Å)	Energy (eV)	ΔE (eV)	Magnetic Momentum (μ_B)	d_{c-c} (Å)	Δd_{c-c} (Å)	Charge Transfer (e)
Graphene	-	-	12.339	-462.874	-	0.000	-	0	-
BLG	AA	-	12.337	-927.804	-2.056	0.000	3.656	0	-
	AB	-	12.336	-928.065	-2.308	0.000	3.486	0	-
Graphite	AA	-	12.337	-928.351	-2.604	0.000	3.621	0	-
	AB	-	12.336	-928.939	-3.120	0.000	3.485	0	-
FeCl ₃	-	FM	12.316	-122.800	-	40.000	-	-	-
		AFM	12.316	-122.817	-	0.000	-	-	-
FeCl ₃ -BLG	AA	FM	12.331	-1053.586	-2.982	39.006	9.550	0.007/0.011	0.982
		AFM	12.332	-1053.571	-2.950	1.001	9.549	0.007/0.010	0.975
	AB	FM	12.332	-1053.579	-2.714	39.005	9.567	0.010/0.026	0.984
		AFM	12.332	-1053.572	-2.690	1.001	9.563	0.006/0.025	0.975
FeCl ₃ -GIC	AB	FM	12.333	-2112.323	-4.422	78.001	9.510	0.005/0.035	2.003
		AFM	12.333	-2112.323	-4.405	0.000	9.510	0.005/0.035	1.985
		AFM2	12.333	-2112.357	-4.439	2.000	9.510	0.005/0.034	1.968

In terms of magnetic stability, the ferromagnetic (FM) state was found to be more stable than the antiferromagnetic (AFM) state for both AA and AB stacking, with energy differences of 15.2 meV and 7.4 meV, respectively. The distances between the two carbon atomic layers varied due to the different positions of Fe and Cl on the stacking carbon layers. It is noticeable that, for AB stacking, the AFM state exhibited slightly smaller d_{c-c} values compared to the FM state, while the difference is not significant for AA stacking.

Furthermore, we investigated the structural changes in the system after intercalation by considering the FM alignment and AA stacking of FeCl₃-intercalated BLG, as it exhibits lowest energy. Each Fe atom forms bonds with six Cl atoms, and the average Fe-Cl bond length around each Fe remains relatively unchanged compared to FeCl₃ monolayer at approximately 2.42 Å. However, there is an exception for a specific Fe atom, where the average Fe-Cl bond length is enlarged to 2.48 Å. A distinct localization of electrons on this Fe atom is evident, gaining around 0.245 electrons. The detailed analysis of the electronic properties of the system will be discussed below.

As shown in Table 1, we quantified the changes in the z-coordinate of carbon atoms in the carbon atomic layers after the intercalation by calculating the difference between the highest and lowest z-coordinate values. The calculation results demonstrate that the intercalations yields a small buckling of the graphene layers, whereas the bending in the AB stacking is about doubly as large as for the AA stacking. Additionally, GIC exhibits even a larger change in the z-coordinate of carbon atoms compared to FeCl₃-intercalated BLG.

3.2. Magnetic and Electronic Properties

The partial density of states (PDOS) and band structure of FeCl₃-intercalated BLG were calculated using the PBE+U+D3 method. Figures A1 and 2 depict the results of the density of states (DOS) for spin-up and spin-down components, respectively. The distinct separation between the spin-up and spin-down DOS peaks indicates a FM coupling in both AA and AB stacking configurations of FeCl₃-intercalated BLG. This leads to a total magnetic

moment of $39 \mu_B$. Conversely, the DOS for the AFM configurations of FeCl_3 -intercalated BLG with both AA and AB stacking exhibit symmetric profiles, resulting in a total magnetic moment of $1 \mu_B$. The states near the Fermi level predominantly originate from Fe $3d$ and Cl $3p$ orbitals.

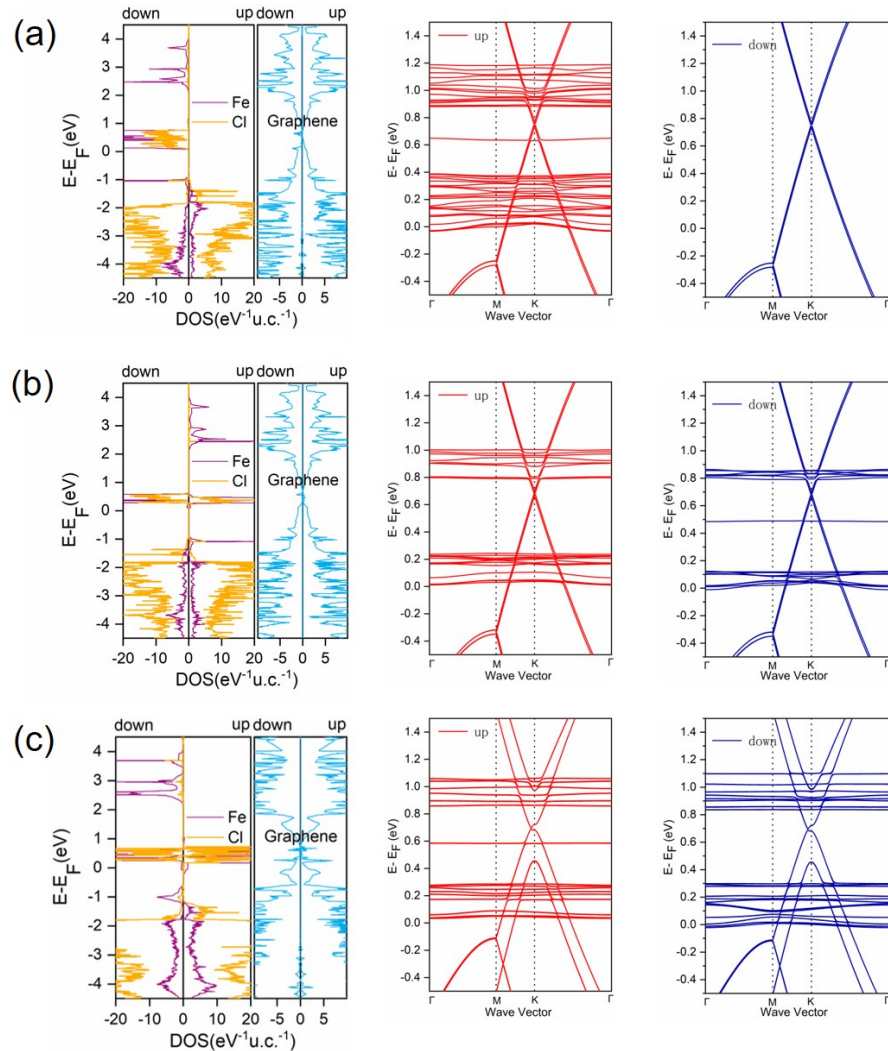


Figure 2. Atom-projected density of states (PDOS) and band structure (spin up component in red and spin down component in blue) obtained for (a) AB stacking FM FeCl_3 -intercalated BLG, (b) AB stacking AFM FeCl_3 -intercalated BLG, and (c) stage-2 AFM2 FeCl_3 -intercalated graphite.

The shift of the Dirac point can be observed for all structures with values of 0.737 eV for AA-FM, 0.682 eV for AA-AFM, 0.750 eV for AB-FM, and 0.676 eV for AB-AFM FeCl_3 -intercalated BLG. The bands near the Dirac points at the K point exhibit a distinct linear dispersion characteristic of the π bands, which closely resembles that of single-layer graphene. Thus, we can conclude that the carbon atomic layers in FeCl_3 -intercalated BLG demonstrate similar electronic properties to those of single-layer graphene.

We further calculated the structural, electronic, and magnetic properties of stage-2 FeCl_3 -intercalated graphite, where adjacent graphene retains AB stacking as in pristine graphite is used for comparison, as it shows the same chemical formula $\text{C}_{12.5}\text{FeCl}_3$ with the FeCl_3 -intercalated BLG. We considered different magnetic configurations (see Table 1), and found that FM order within the FeCl_3 layer and AFM order between the planes (named AFM2) has the lowest energy; therefore, we will discuss the electronic and structural properties only for this magnetic arrangement.

The optimized lattice constant a and c are equal to 12.333 and 26.032 Å, respectively. The distance between the two graphene layers is approximately 9.510 Å for the stage-2 GIC, which is somewhat smaller than the BLG by 0.04 Å. This result is expected, since in BLG, the graphene layers can relax to the vacuum region. FeCl₃-intercalated graphite exhibits a more significant variation in the z -coordinate of carbon atoms compared to FeCl₃-intercalated BLG. Additionally, in FeCl₃ layers, a specific Fe atom shows an enlargement of the average Fe-Cl bond length, with a value of 2.48 Å, which is consistent with the behavior observed in the BLG system. The calculated intercalation energy is around -8.879 eV for the system, which corresponds to an energy of -0.555 eV per FeCl₃ unit, which is significantly larger than in BLG. As shown in Figure 2c, the symmetric DOS suggest AFM coupling for stage-2 intercalated graphite and an up shift of the Dirac point of 0.695 eV can be observed on the band structure, which is slightly lower than for the BLG.

We further investigated the charge transfer between FeCl₃ and carbon atomic layer of FeCl₃-intercalated BLG and FeCl₃-intercalated graphite. As shown in Figure 3, it is clear that the hole is delocalized within the graphene layers. The charge transfer in BLG (per FeCl₃ layer) is slightly smaller than the stage-2 intercalated graphite, owing to the absence of the graphene layers on top and down side of the FeCl₃-intercalated BLG. However, it is intriguing to note that the partial charges of the majority of Fe atoms remain largely unaffected, while a distinct localization of electrons on a specific Fe atom is evident, gaining approximately 0.245 electrons determined by the Bader analysis. Meanwhile, the 6 Cl atoms that bond with this Fe also undergo similar changes, gaining a total of 0.282 electrons, while the remaining 18 Cl atoms collectively gain 0.389 electrons (Figure 3a). Similar behavior is observed in FeCl₃ GIC, where in each layer, one Fe atom gains 0.245 electrons, and the 6 Cl atoms bonded to this specific Fe gain a total of 0.273 electrons, while the remaining 18 Cl atoms collectively gain 0.405 electrons.

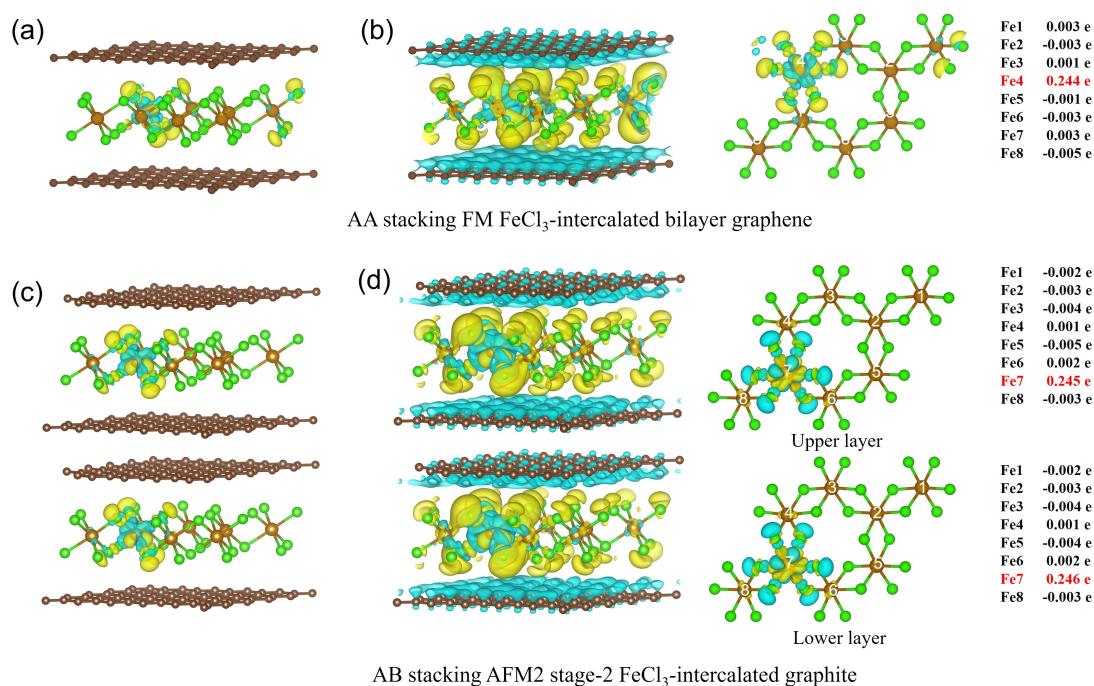


Figure 3. Superimposed with electron density redistribution calculation results and individual charge difference of Fe in intercalation system compared to FeCl₃ monolayer: $\Delta\rho(\mathbf{r}) = \rho_{A/B}(\mathbf{r}) - [\rho_A(\mathbf{r}) + \rho_B(\mathbf{r})]$ (A: carbon atomic layers; B: FeCl₃). Here, $\Delta\rho(\mathbf{r})$ is color coded as blue ($-0.002 e \text{ \AA}^{-3}$), white (0), yellow ($+0.002 e \text{ \AA}^{-3}$) in (a,c); and as blue ($-0.0005 e \text{ \AA}^{-3}$), white (0), yellow ($+0.0005 e \text{ \AA}^{-3}$) in (b,d).

3.3. Pressure Dependence

Within the bilayer system, we can apply uniaxial pressure perpendicular to the 2D system to investigate whether the magnetic state can be modulated by pressure. As shown in Table 2, we create the pressure by adjusting the interlayer spacing between the graphene layers while keeping the FeCl₃ layer equally spaced from both. In the calculation, the z coordinates of the system were constrained, preventing relaxation along the vertical direction. However, the atoms retained the freedom to move within the xy plane, allowing for structural optimizations within that plane. The energy for both the FM and AFM states of FeCl₃-intercalated BLG is determined at every interval of 0.1 Å when the interlayer spacing is changed from 9.5 to 9.0 Å.

Table 2. Energies for FM and AFM states, shift of Dirac point, and charge transfer occurring from graphene to FeCl₃ with varying interlayer distances for FeCl₃ intercalated BLG.

d_{C-C} (Å)	E_{FM} (eV)	Shift of Dirac Point/ Charge Transfer Value	E_{AFM} (eV)	Shift of Dirac Point/ Charge Transfer Value
9.5	−1053.572	0.7579/0.9907	−1053.549	0.6919/0.9799
9.4	−1053.521	0.7648/0.9988	−1053.498	0.7021/0.9865
9.3	−1053.448	0.7666/1.0144	−1053.429	0.7065/0.9993
9.2	−1053.330	0.7734/1.0247	−1053.306	0.7180/1.0033
9.1	−1053.151	0.7740/1.0391	−1053.124	0.7249/1.0134
9.0	−1052.915	0.7753/1.0579	−1052.886	0.7259/1.0307

Based on the calculation results, it can be concluded that in all studied structures, FeCl₃-intercalated BLG exhibits greater stability in the FM state compared to the AFM state. The energy difference between the two states is approximately 25 meV for the system. This suggests that, even under pressure, the magnetic state of the FeCl₃-intercalated BLG is independent of the pressure applied. The applied pressure increases the charge transfer and the shift of the Dirac point slightly, but the important finding is that not only the magnetic properties, but also the electronic properties, remain stable under applied pressure.

4. Conclusions

In summary, our calculations revealed that a distinct localization of electrons on a specific Fe atom is evident, gaining approximately 0.245 electrons, and its surrounding chlorides gain 0.282 electrons in total. The holes are delocalized within the carbon atomic layers with a positive charge of around 0.01 eV per carbon. Consequently, the intercalated graphene exhibits p-type doping, leading to a shift of the Dirac cone by 0.74 eV for BLG and 0.70 eV for stage-2 intercalated graphite. Moreover, our calculations indicate the presence of ferromagnetic ordering within the plane of FeCl₃-intercalated BLG, while the FeCl₃ layers in stage-2 intercalated graphite exhibit antiferromagnetic coupling. The ferromagnetic nature and the charge transfer remains stable under pressure. This stable high charge transfer from the carbon layers and the significant shift of the Dirac point, whereas the linear dispersion relations are preserved, suggests that FeCl₃-intercalated BLG holds promising potential for future advances in low-dimensional electronics.

Author Contributions: Conceptualization, B.P. and J.D.; methodology, J.D. and S.Y.; writing—original draft preparation, J.D.; writing—review and editing, B.P.; supervision, B.P. All authors have read and agreed to the published version of the manuscript.

Funding: This research was funded by Freie Universität Berlin.

Data Availability Statement: Data are contained within the article.

Acknowledgments: J.D. acknowledges the China Scholarship Council for their financial support. The computing time granted by the Resource Allocation Board and provided on the supercomputer Lise and Emmy at NHR@ZIB and NHR@Göttingen as part of the NHR infrastructure is gratefully acknowledged.

Conflicts of Interest: The authors declare no conflict of interest.

Abbreviations

The following abbreviations are used in this manuscript:

DFT	Density functional theory
BLG	Bilayer graphene
SLG	Single-layer graphene
FLG	Few-layer graphene
GICs	Graphite intercalation compounds
DOS	Density of state

Appendix A

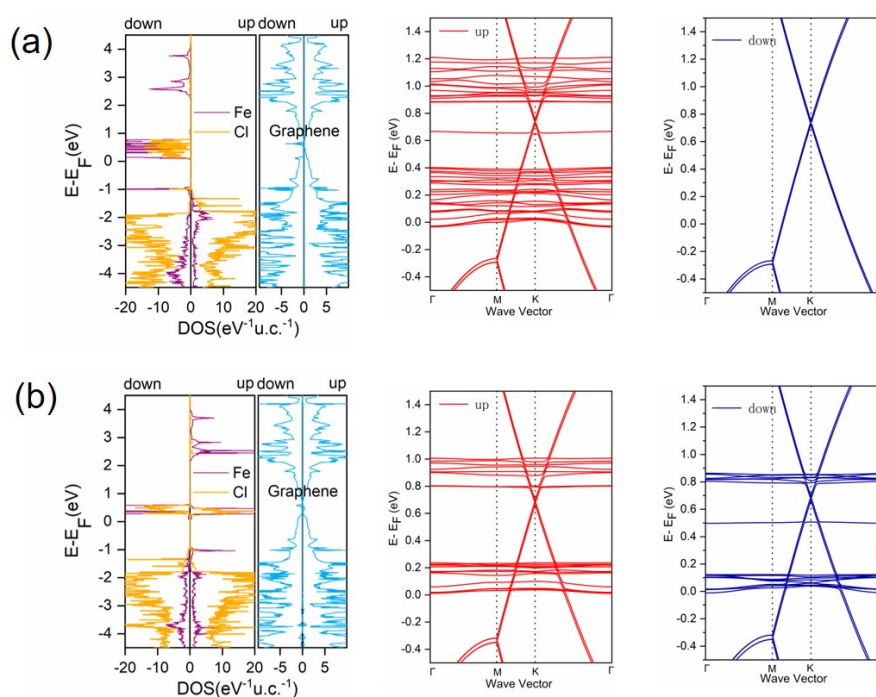


Figure A1. Site-projected density of states (PDOS) and band structure (spin up component in red and spin down component in blue) obtained for (a) AA stacking FM FeCl_3 -intercalated BLG and (b) AA stacking AFM FeCl_3 -intercalated BLG.

References

- Rüdorff, W. Graphite intercalation compounds. In *Advances in Inorganic Chemistry and Radiochemistry*; Elsevier: Amsterdam, The Netherlands, 1959; Volume 1, pp. 223–266.
- Selig, H.; Ebert, L.B. Graphite intercalation compounds. In *Advances in Inorganic Chemistry and Radiochemistry*; Elsevier: Amsterdam, The Netherlands, 1980; Volume 23, pp. 281–327.
- Nobuhara, K.; Nakayama, H.; Nose, M.; Nakanishi, S.; Iba, H. First-principles study of alkali metal-graphite intercalation compounds. *J. Power Sources* **2013**, *243*, 585–587. [[CrossRef](#)]
- Dresselhaus, M.S. Intercalation in layered materials. *MRS Bull.* **1987**, *12*, 24–28. [[CrossRef](#)]
- Besenhart, J. The electrochemical preparation and properties of ionic alkali metal-and NR_4 -graphite intercalation compounds in organic electrolytes. *Carbon* **1976**, *14*, 111–115. [[CrossRef](#)]
- Pruvost, S.; Hérold, C.; Hérold, A.; Lagrange, P. Co-intercalation into graphite of lithium and sodium with an alkaline earth metal. *Carbon* **2004**, *42*, 1825–1831. [[CrossRef](#)]
- Dresselhaus, M.S.; Dresselhaus, G. Intercalation compounds of graphite. *Adv. Phys.* **2002**, *51*, 1–186. [[CrossRef](#)]
- Noel, M.; Santhanam, R. Electrochemistry of graphite intercalation compounds. *J. Power Sources* **1998**, *72*, 53–65. [[CrossRef](#)]
- Jiang, H. Chemical preparation of graphene-based nanomaterials and their applications in chemical and biological sensors. *Small* **2011**, *7*, 2413–2427. [[CrossRef](#)] [[PubMed](#)]

10. Kim, W.S.; Moon, S.Y.; Bang, S.Y.; Choi, B.G.; Ham, H.; Sekino, T.; Shim, K.B. Fabrication of graphene layers from multiwalled carbon nanotubes using high dc pulse. *Appl. Phys. Lett.* **2009**, *95*, 083103. [[CrossRef](#)]
11. Novoselov, K.S.; Geim, A.K.; Morozov, S.V.; Jiang, D.; Katsnelson, M.I.; Grigorieva, I.V.; Dubonos, S.; Firsov, A.A. Two-dimensional gas of massless Dirac fermions in graphene. *Nature* **2005**, *438*, 197–200. [[CrossRef](#)]
12. Wang, H.; Strait, J.H.; George, P.A.; Shivaraman, S.; Shields, V.B.; Chandrashekhar, M.; Hwang, J.; Rana, F.; Spencer, M.G.; Ruiz-Vargas, C.S.; et al. Ultrafast relaxation dynamics of hot optical phonons in graphene. *Appl. Phys. Lett.* **2010**, *96*, 081917. [[CrossRef](#)]
13. Kampfrath, T.; Perfetti, L.; Schapper, F.; Frischkorn, C.; Wolf, M. Strongly coupled optical phonons in the ultrafast dynamics of the electronic energy and current relaxation in graphite. *Phys. Rev. Lett.* **2005**, *95*, 187403. [[CrossRef](#)]
14. Graf, D.; Molitor, F.; Ensslin, K.; Stampfer, C.; Jungen, A.; Hierold, C.; Wirtz, L. Spatially resolved Raman spectroscopy of single- and few-layer graphene. *Nano Lett.* **2007**, *7*, 238–242. [[CrossRef](#)] [[PubMed](#)]
15. Lui, C.H.; Li, Z.; Chen, Z.; Klimov, P.V.; Brus, L.E.; Heinz, T.F. Imaging stacking order in few-layer graphene. *Nano Lett.* **2011**, *11*, 164–169. [[CrossRef](#)]
16. Wei, D.; Wu, B.; Guo, Y.; Yu, G.; Liu, Y. Controllable chemical vapor deposition growth of few layer graphene for electronic devices. *Accounts Chem. Res.* **2013**, *46*, 106–115. [[CrossRef](#)]
17. Orsu, P.; Koyyada, A. Recent progresses and challenges in graphene based nano materials for advanced therapeutical applications: a comprehensive review. *Mater. Today Commun.* **2020**, *22*, 100823. [[CrossRef](#)]
18. Zhang, H.; Feng, P.X. Fabrication and characterization of few-layer graphene. *Carbon* **2010**, *48*, 359–364. [[CrossRef](#)]
19. Zhang, L.; Zhang, Z.; He, C.; Dai, L.; Liu, J.; Wang, L. Rationally designed surfactants for few-layered graphene exfoliation: ionic groups attached to electron-deficient π -conjugated unit through alkyl spacers. *ACS Nano* **2014**, *8*, 6663–6670. [[CrossRef](#)] [[PubMed](#)]
20. Nijamudheen, A.; Sarbapalli, D.; Hui, J.; Rodríguez-López, J.; Mendoza-Cortes, J.L. Impact of surface modification on the lithium, sodium, and potassium intercalation efficiency and capacity of few-layer graphene electrodes. *ACS Appl. Mater. Interfaces* **2020**, *12*, 19393–19401. [[CrossRef](#)]
21. McCann, E.; Koshino, M. The electronic properties of bilayer graphene. *Rep. Prog. Phys.* **2013**, *76*, 056503. [[CrossRef](#)]
22. Ohta, T.; Bostwick, A.; Seyller, T.; Horn, K.; Rotenberg, E. Controlling the electronic structure of bilayer graphene. *Science* **2006**, *313*, 951–954. [[CrossRef](#)]
23. Zhao, W.; Tan, P.H.; Liu, J.; Ferrari, A.C. Intercalation of few-layer graphite flakes with FeCl₃: Raman determination of Fermi level, layer by layer decoupling, and stability. *J. Am. Chem. Soc.* **2011**, *133*, 5941–5946. [[CrossRef](#)]
24. Sun, Y.; Han, F.; Zhang, C.; Zhang, F.; Zhou, D.; Liu, H.; Fan, C.; Li, X.; Liu, J. FeCl₃ Intercalated microcrystalline graphite enables high volumetric capacity and good cycle stability for lithium-ion batteries. *Energy Technol.* **2019**, *7*, 1801091. [[CrossRef](#)]
25. Millman, S.; Holmes, B.; Zimmerman, G. Magnetic susceptibility study of magnetic properties in low stage FeCl₃ intercalated graphite. *Solid State Commun.* **1982**, *43*, 903–906. [[CrossRef](#)]
26. Kim, N.; Kim, K.S.; Jung, N.; Brus, L.; Kim, P. Synthesis and electrical characterization of magnetic bilayer graphene intercalate. *Nano Lett.* **2011**, *11*, 860–865. [[CrossRef](#)]
27. Nathaniel, J.; Wang, X.Q. Tunable electron and hole doping in FeCl₃ intercalated graphene. *Appl. Phys. Lett.* **2012**, *100*, 213112. [[CrossRef](#)]
28. Bonacum, J.P.; O'Hara, A.; Bao, D.L.; Ovchinnikov, O.S.; Zhang, Y.F.; Gordeev, G.; Arora, S.; Reich, S.; Idrobo, J.C.; Haglund, R.F.; et al. Atomic-resolution visualization and doping effects of complex structures in intercalated bilayer graphene. *Phys. Rev. Mater.* **2019**, *3*, 064004. [[CrossRef](#)]
29. Zhan, D.; Sun, L.; Ni, Z.H.; Liu, L.; Fan, X.F.; Wang, Y.; Yu, T.; Lam, Y.M.; Huang, W.; Shen, Z.X. FeCl₃-based few-layer graphene intercalation compounds: single linear dispersion electronic band structure and strong charge transfer doping. *Adv. Funct. Mater.* **2010**, *20*, 3504–3509. [[CrossRef](#)]
30. Zou, X.; Zhan, D.; Fan, X.; Lee, D.; Nair, S.K.; Sun, L.; Ni, Z.; Luo, Z.; Liu, L.; Yu, T.; et al. Ultrafast carrier dynamics in pristine and FeCl₃-intercalated bilayer graphene. *Appl. Phys. Lett.* **2010**, *97*, 141910. [[CrossRef](#)]
31. Li, Y.; Yue, Q. First-principles study of electronic and magnetic properties of FeCl₃-based graphite intercalation compounds. *Phys. B Condens. Matter* **2013**, *425*, 72–77. [[CrossRef](#)]
32. Kresse, G.; Furthmüller, J. Efficient iterative schemes for ab initio total-energy calculations using a plane-wave basis set. *Phys. Rev. B* **1996**, *54*, 11169. [[CrossRef](#)]
33. Kresse, G.; Joubert, D. From ultrasoft pseudopotentials to the projector augmented-wave method. *Phys. Rev. B* **1999**, *59*, 1758. [[CrossRef](#)]
34. Perdew, J.P.; Burke, K.; Ernzerhof, M. Generalized gradient approximation made simple. *Phys. Rev. Lett.* **1996**, *77*, 3865. [[CrossRef](#)]
35. Blöchl, P.E. Projector augmented-wave method. *Phys. Rev. B* **1994**, *50*, 17953. [[CrossRef](#)]
36. Blöchl, P.E.; Jepsen, O.; Andersen, O.K. Improved tetrahedron method for Brillouin-zone integrations. *Phys. Rev. B* **1994**, *49*, 16223. [[CrossRef](#)]
37. Anisimov, V.I.; Aryasetiawan, F.; Lichtenstein, A. First-principles calculations of the electronic structure and spectra of strongly correlated systems: The LDA+ U method. *J. Phys. Condens. Matter* **1997**, *9*, 767. [[CrossRef](#)]
38. Dudarev, S.L.; Botton, G.A.; Savrasov, S.Y.; Humphreys, C.; Sutton, A.P. Electron-energy-loss spectra and the structural stability of nickel oxide: An LSDA+ U study. *Phys. Rev. B* **1998**, *57*, 1505. [[CrossRef](#)]

39. Grimme, S.; Antony, J.; Ehrlich, S.; Krieg, H. A consistent and accurate ab initio parametrization of density functional dispersion correction (DFT-D) for the 94 elements H-Pu. *J. Chem. Phys.* **2010**, *132*, 154104. [[CrossRef](#)] [[PubMed](#)]
40. Yu, M.; Trinkle, D.R. Accurate and efficient algorithm for Bader charge integration. *J. Chem. Phys.* **2011**, *134*, 064111. [[CrossRef](#)] [[PubMed](#)]

Disclaimer/Publisher's Note: The statements, opinions and data contained in all publications are solely those of the individual author(s) and contributor(s) and not of MDPI and/or the editor(s). MDPI and/or the editor(s) disclaim responsibility for any injury to people or property resulting from any ideas, methods, instructions or products referred to in the content.